HHS Public Access

Author manuscript

Adv Funct Mater. Author manuscript; available in PMC 2021 March 17.

Published in final edited form as:

Adv Funct Mater. 2020 March 17; 30(12): . doi:10.1002/adfm.201908961.

Inhibition of Immunosuppressive Tumors by Polymer-Assisted Inductions of Immunogenic Cell Death and Multivalent PD-L1 Crosslinking

Lian Li,
Department of Pharmaceutics and Pharmaceutical Chemistry/Center for Controlled Chemical Delivery, University of Utah, Salt Lake City, Utah 84112, USA

Yachao Li,
Department of Pharmaceutics and Pharmaceutical Chemistry/Center for Controlled Chemical Delivery, University of Utah, Salt Lake City, Utah 84112, USA

Chieh-Hsiang Yang,
Department of Biomedical Engineering, University of Utah, Salt Lake City, Utah 84112, USA

D. Christopher Radford,
Department of Biomedical Engineering, University of Utah, Salt Lake City, Utah 84112, USA

Jiawei Wang,
Department of Pharmaceutics and Pharmaceutical Chemistry/Center for Controlled Chemical Delivery, University of Utah, Salt Lake City, Utah 84112, USA

Margit Janát-Amsbury,
Department of Pharmaceutics and Pharmaceutical Chemistry/Center for Controlled Chemical Delivery, University of Utah, Salt Lake City, Utah 84112, USA

Jindřich Kopeček,
Department of Pharmaceutics and Pharmaceutical Chemistry/Center for Controlled Chemical Delivery, University of Utah, Salt Lake City, Utah 84112, USA

Department of Biomedical Engineering, University of Utah, Salt Lake City, Utah 84112, USA

Jiyuan Yang
Department of Pharmaceutics and Pharmaceutical Chemistry/Center for Controlled Chemical Delivery, University of Utah, Salt Lake City, Utah 84112, USA

Abstract

Checkpoint blockade immunotherapies harness the host's own immune system to fight cancer, but only work against tumors infiltrated by swarms of pre-existing T cells. Unfortunately, most

jindrich.kopecek@utah.edu, jiyuan.yang@utah.edu.

Conflict of Interest

J.K. and J.Y. are co-inventors of US Patent 9,289,510 related to KT-1; L.L., J.K., and J.Y. are co-inventors of a patent application related to combination chemo- and immunotherapy. The University of Utah licensed both to TheraTarget. Inc.

Supporting Information

Supporting Information is available from the Wiley Online Library or from the authors.

cancers to date are immune-deserted. Here, we report a polymer-assisted combination of immunogenic chemotherapy and PD-L1 degradation for efficacious treatment in originally non-immunogenic cancer. “Priming” tumors with backbone-degradable polymer-epirubicin conjugates elicits immunogenic cell death and fosters tumor-specific CD8+ T cell response. Sequential treatment with a multivalent polymer-peptide antagonist to PD-L1 overcomes adaptive PD-L1 enrichment following chemotherapy, biases the recycling of PD-L1 to lysosome degradation *via* surface receptor crosslinking, and produces prolonged elimination of PD-L1 rather than the transient blocking afforded by standard anti-PD-L1 antibodies. Together, these findings established the polymer-facilitated tumor targeting of immunogenic drugs and surface crosslinking of PD-L1 as a potential new therapeutic strategy to propagate a long-term antitumor immunity, which might broaden the application of immunotherapy to immunosuppressive cancers.

Keywords

checkpoint blockade immunotherapy; immunosuppressive tumor; immunogenic cell death; PD-L1 crosslinking; HPMA polymer

1. Introduction

After chemotherapy cessation, residual tumor cells may adaptively upregulate programmed death-1 (PD-1) ligand 1 (PD-L1) to interact with immune checkpoint receptor PD-1 on T cells, creating an immunosuppressive state to escape immunosurveillance.[1] In contrast, PD-L1 blockade therapies unleash the function of pre-existing tumor-infiltrating T cells, inhibit cancer durably, but do not benefit a majority of patients with immune-deserted tumors which are, for various reasons, devoid of tumor-reactive CD8+ T cells or do not provoke strong immune response.[2] Thus, a great challenge lies in applying immunotherapy to immunosuppressive cancers.

To transform immune-deserted tumors into immune-cultivated ones displaying antitumor T cell immunity, one approach might involve the immunogenic cell death (ICD)-inducing modalities.[3] In contrast to most other cytotoxic chemotherapeutics, anthracyclines (*e.g.* epirubicin and doxorubicin) not only kill cancer cells directly but also instigate a cascade of ICD events (*e.g.* preapoptotic exposure of calreticulin and postapoptotic release of high mobility group box 1) that favor the engulfment of dying cells by antigen-presenting cells and ultimately recruit T cell engagement.[4]. However, anthracyclines are low molecular drugs with off-target issues.[5] 1st generation *N*-(2-hydroxypropyl)methacrylamide (HPMA) polymer-bound anthracyclines target tumors, and decrease adverse effects.[6] To further enhance tumor accumulation, 2nd generation HPMA copolymer-anticancer drug conjugates have been developed, with higher molecular weight to extend blood circulation and insertion of enzymatically degradable oligopeptide sequences into the backbone to guarantee biocompatibility.[7] The leading backbone degradable conjugate is KT-1, HPMA copolymer-epirubicin (EPI) conjugate (also known as 2P-EPI). Mounting evidence suggests that KT-1 possesses significantly superior pharmacokinetics and preferential tumor biodistribution over free EPI and 1st generation conjugates. But whether KT-1 can generate vaccine-like functions to render tumor immunogenic and collaborate with immunotherapy is unknown.

Another challenge in prevalent anti-PD-L1 antibody (α-PD-L1) treatment is that tumor cells continue to maintain the extracellular expression of PD-L1 even after the conformational blockade on cell membrane. Recent findings suggest PD-L1 is actively recycled and repopulated to cell surface after dragging α-PD-L1 into cells.[8] To prevent unwanted PD-L1 recycling, controlled trafficking of PD-L1 to targeted degradation in the lysosomes might be a key, as exemplified by several recent studies: CMTM6 protein depletion triggers endocytosed PD-L1 to detour for lysosome and alleviates T cell suppression;[8a] a fusion peptide incorporating a PD-L1-binding sequence and lysosome-sorting signal governs lysosomal localization of PD-L1 and depletes PD-L1;[8b] inhibiting PD-L1 palmitoylation leads PD-L1 degradation in the lysosomes and enhances T-cell immune responses against tumors.[8c]

Inspired by the findings of surface receptor crosslinking as a universal method to manipulate subcellular targeting of receptor-bound ligands to lysosomes,[9] we envision crosslinking PD-L1 would trigger its clearance in lysosomes and exhibit significant therapeutic benefit, which is not yet reported. To this end, linear HPMA copolymer with multiple copies of binding motifs might be advantageous for the receptor crosslinking, because the random coil conformation facilitates to better present targeting moieties and the multivalence enables the capacity to simultaneously crosslink numerous targeted receptors.[10] Previously, we demonstrated CD20 receptor crosslinking by HPMA copolymer-based therapeutic directs CD20 to lysosome and inhibits its surface recycling.[11]

Here, we describe a polymer-based two-wave strategy that consists of (i) immunogenic chemotherapy: long-circulating epirubicin conjugate KT-1, and (2) PD-L1 degradation immunotherapy: multivalent HPMA polymer-peptide antagonists to PD-L1 (MPPA). We hypothesize the 1st strike of KT-1 specifically targets and immunologically “heats up” tumor *via* inducing ICD. The 2nd strike of MPPA blocks PD-1/PD-L1 interaction and biases the recycling of PD-L1 to lysosome degradation *via* multivalent receptor crosslinking (Figure 1). By these efforts, the 1st strike of chemotherapy is expected to prime anti-cancer immunity and potentiate the 2nd strike of immunotherapy to efficiently eliminate established tumors and prevent tumor relapse.

2. Results

2.1 KT-1 enhances drug delivery and triggers immunogenic cell death

Detailed synthesis routes and characterizations of the conjugates KT-1 and MPPA are presented in Figure S1–4, Supporting Information. KT-1, a degradable diblock HPMA copolymer-EPI conjugate with narrow polydispersity, was synthesized *via* one step reversible addition-fragmentation chain transfer polymerization and characterized in Figure S1, Supporting Information. Previously, we demonstrated KT-1 drastically prolonged systemic circulating half-life (33.2±3.2 h) as compared with free drug (~16 min).[7] Here, we also validated KT-1 has long-lasting retention in tumors. 4T1, murine triple-negative breast cancer cell line sharing genomic feathers of basal-like breast cancer which is known to be a non-immunogenic tumor with clinical objective response rate<20%, was selected as the syngeneic cancer model.[1a] As shown in Figure 2A, cyanine5 (Cy5), a fluorescent tracer with similar molecular weight and hydrophobicity as EPI, was rapidly eliminated from the

tumor and barely detectable after 2 h post injection. In contrast, KT-1-Cy5 profoundly accumulated at tumor site, which peaked at 24 h and lasted for at least 196 h. As a result, KT-1 drastically enhanced tumor cell uptake of EPI *in vivo* (Figure 2B).

Having shown tumor-targeted delivery of KT-1, we next examined its impact on inducing ICD that implicates calreticulin (CRT) expression and high-mobility group box 1 (HMGB1) protein release. CRT exposed on the surfaces of immunogenically dying tumor cells sends dendritic cells (DCs) an “eat me” signal to facilitate phagocytosis by antigen-presenting cells (APCs), while released HMGB1 functions as the “danger” signal and stimulates optimal antigen presentation to T cells.[3,4] KT-1 triggered significant upregulation of surface CRT and HMGB1 *in vitro* (Figure 2C; Figure S5, Supporting Information), which was induced by the intracellular delivery of EPI, but not polymer backbone. In Figure 2D, E, BALB/c mice bearing non-immunogenic 4T1 tumors, were given two intravenous doses (on Day 7 and 14 after tumor implantation) of treatments with saline, EPI or KT-1 (first EPI equivalence dose 10 mg/kg followed by second dose 5 mg/kg). Analysis on Day 15 revealed KT-1 treatment enhanced the CRT expression on 4T1 cells (Figure 2D) and intratumoral release of HMGB1 (Figure 2E) as compared with free EPI, which corresponds with greater tumor accumulation of KT-1 *in vivo*.

Notably, compared with mice treated with free EPI, KT-1-treated mice had a higher frequency of F4/80-CD11c+CD11b−/+ DCs within tumors (Figure 2F). It was reported that tumor-infiltrating DCs (TIDCs), when activated, are a subset of potent APCs that are fully competent to process tumor antigens and prime T cells.[12] To assess the functional status of TIDCs, we analyzed their surface expression of the activation markers, major histocompatability (MHC) class II proteins and the costimulatory molecule CD86. As shown in Figure 2G, TIDCs in KT-1-treated tumors exhibited significant up-regulations of MHC II and CD86, as compared with the control groups treated with saline and free EPI. This could be the result of efficiently triggering ICD-associated signals by KT-1 in tumors, which sequentially attracts DCs into tumor bed, stimulates phagocytosis of the dying tumor cells by DCs, and matures DCs endowing them with the ability to activate tumor-specific T cells. As a result, KT-1 recruited drastically higher frequency of CD8+ T cells into the tumor bed than free EPI (Figure 2H).

2.2 KT-1 elicits CD8+ T cell-dependent tumor inhibition and adaptive increase in PD-L1 expression

Having demonstrated KT-1-triggered ICD responses, we evaluated whether it could translate into improved therapeutic efficacy *in vivo*. BALB/c mice were inoculated with 4T1 cells, and given 3 rounds of weekly treatment with saline, EPI and KT-1 (first EPI equivalence dose10 mg/kg followed by two doses 5 mg/kg). As shown in Figure 3A, B and Figure S6A, Supporting Information, all saline treated mice experienced explosive tumor growth and died rapidly. EPI at this dose had limited effect on controlling tumor or extending survival. Of note, KT-1 treatment significantly suppressed the tumor growth and improved animal survival rate.

To clarify whether the tumor control solely depends on direct drug actions or also requires CD8+ T lymphocytes, 4T1-tumor bearing mice were subjected to CD8+ T-cell ablation

using CD8-depleting antibodies during the KT-1 treatment. The result showed concurrent depletion of CD8+ T cells markedly weakened KT-1-mediated tumor regression (Figure 3C; Figure S6B, Supporting Information) and compromised mice survival (Figure 3D), suggesting KT-1 inhibits tumor progression through a CD8+ T cell-dependent manner.

As expected, at the endpoint of above treatments, we found KT-1 treatment fostered CD8+ T cell infiltration into tumors (Figure 3E, F). However, Tregs that hamper effective anti-tumor immune responses did not alter among all treated groups (Figure 3E, G). Although KT-1 significantly promotes the overall CD8+ T cells to Treg ratio to improve antitumor immunity (Figure 3H), it still failed to completely eradicate the tumors in mice (Figure 3A). Correlating with other reports following chemotherapy,[1] we also found PD-L1 expression adaptively enriched in both EPI and KT-1 treated tumors (Figure 3I), which could be due to the negative feedback mechanisms that followed $CD8^+$ T cell infiltration.[13] The increment of tumoral PD-L1, together with unaffected presence of Tregs in tumor microenvironment, may reflect the multiple immunosuppressive mechanisms employed by the residual cancer cells against chemotherapy, and highlight the necessity of further combining with PD-L1 blockade.

To evaluate the therapeutic potential of KT-1 combining with PD-L1 blockade, BALB/c mice were treated as shown in Figure 3J. Mice did not respond to α-PD-L1 monotherapy, largely due to the lack of PD-L1 expression and T cell engagement in 4T1 tumors. Free EPI combining with α-PD-L1 (EPI→α-PD-L1) delayed the tumor growth only marginally. In stark contrast, KT-1→α-PD-L1 therapy exerted remarkable tumor regression, eliminating established tumors in 80% of mice, and achieved a dramatic 100% animal survival (Figure 3K; Figure S6C, Supporting Information). These results suggest, by efficiently delivering EPI to tumor, KT-1 was able to render unresponsive tumors immunogenic and sensitive to PD-L1 blockade.

2.3 MPPA targets PD-L1 to lysosomal degradation

Given emerging evidence indicating surface PD-L1 can be rapidly recycled and restored after α-PD-L1 binding,[8] it is imperative to not only bind PD-L1 on cell surface but also eliminate it within the cell. To redirect PD-L1 from the recycling pathway to lysosomal degradation, we designed a multivalent polymer-peptide antagonist to PD-L1, which involved the operation of receptor crosslinking as a molecular switch (Figure 4A).

PD-L1 peptide antagonist (PPA), with the amino acid sequence shown in Figure S2A, Supporting Information, was reported to bind PD-L1 with high affinity,[14] and further confirmed in Figure S2B, Supporting Information. To achieve multimeric PD-L1 crosslinking, PPA was grafted onto HPMA copolymer to generate the multivalent polymer-PPA conjugates. The synthetic scheme and conjugate characterizations are presented in Figure S2C, Supporting Information. By varying the ratio of the reaction components, a panel of conjugates was prepared with different valences for subsequent evaluation. Three conjugates with Cy3 labeled backbone were prepared: P-$(PPA)_{14}$-Cy3, P-$(PPA)_{4.3}$-Cy3, P-$(PPA)_{1.3}$-Cy3, where the subscript denotes the valence. Additionally, one unlabeled conjugate (MPPA) for receptor depletion studies was prepared with degradable backbone.

The characterization of MPPA with the PPA valence of 12.6 is presented in Figure S1C, Supporting Information.

Figure S3, Supporting Information shows the surface binding affinity of P-$(PPA)_x$ increased as the valence increased. Consistent with numerous studies that demonstrated receptor crosslinking triggers endocytosis,[9] multivalent P-$(PPA)_{14}$-Cy3 and P-$(PPA)_{4.3}$-Cy3 had accelerated internalization rates as compared with low-valence P-$(PPA)_{1.3}$-Cy3 and polymer precursor P-Cy3 (Figure S4, Supporting Information). Upon specific binding and enhanced internalization driven by PD-L1 crosslinking, we have also demonstrated substantial MPPA internalized into lysosome while lysosome colocalization with α-PD-L1 was partial and limited (Figure 4B). In particular, compared with α-PD-L1 treatment, MPPA resulted in an obvious expansion in lysosome volume and brightness/acidity. This intriguing phenomenon led us to quantitatively examine the mean fluorescent intensity (MFI) of stained lysosomes after various treatments (Figure S7, Supporting Information). Results showed that compared with untreated control, α-PD-L1 and PPA did not alter the MFI of lysosomes while polymer backbone only induced a marginal increment. In contrast, marked enhancement of lysosome MFI was found after MPPA treatment. This could be the result of MPPA-mediated receptor crosslinking. Compared with α-PD-L1 and PPA that only bind to PD-L1 receptor which is actively recycled and repopulated to cell surface, MPPA multivalently crosslinks PD-L1, and biases the recycling of PD-L1 to target lysosomes. Compared with polymer backbone that is passively encapsulated by cell membrane and endocytosed into lysosomes, MPPA exerts accelerated internalization into lysosomes. Enhanced and sometimes aberrant lysosomal delivery has been observed for many receptors when clustered or crosslinked into "supramultivalent" interactions. [9a]As trafficking to lysosomes involves complicated fusions of multiple intracellular vacuolar membranes, lysosomes might be remodeled to accommodate MPPA-mediated PD-L1 crosslinking for targeting lysosome.

MPPA depleted PD-L1 to a higher degree than α-PD-L1 24 h post cell binding, while the presence of E-64, an irreversible, potent, and highly selective cysteine protease inhibitor that partially prevents enzymatic degradation in lysosomes,[15] alleviated PD-L1 depletion by MPPA (Figure 4C). In support of enhanced lysosomal degradation of PD-L1 by MPPA, we found, using recycling assay,[8a] that MPPA treatment resulted in a markedly slow and impaired recovery of surface PD-L1 as compared with α-PD-L1 and PPA (Figure 4D), indicating that increased amount of internalized PD-L1 after MPPA treatment did not recycle back to cell surface and instead were rerouted to the lysosome for degradation. Together, these findings established the polymer-facilitated crosslinking of surface PD-L1 strategy as a potential new therapeutic avenue to produce prolonged elimination of PD-L1, rather than the transient blocking afforded by standard anti-PDL1 antibodies.

We next investigated the tumor targeting efficiency of MPPA (Figure 4E). After 24 h post i.v. injection, considerable accumulation of MPPA was found in tumors, which was significantly higher than in other major organs, especially liver and spleen that abundantly express PD-L1. To validate the capability of MPPA to deplete PD-L1 in tumor, mice bearing 4T1 tumors were treated with α-PD-L1, PPA, or MPPA on Day 15, following two doses of KT-1 treatment on Day 7 and 14 (Figure 4F). Tumoral PD-L1 level and tumor-infiltrating lymphocytes were determined two days post PD-L1 blockade. Consistent with earlier

finding, the overall PD-L1 level in KT-1 treated tumors is adaptively enriched to avoid obliteration by immune T cells. Sequential PD-L1 blockade therapies, α-PD-L1 and PPA, downregulated PD-L1 expression. A further enhanced reduction in PD-L1 expression was achieved by MPPA, which prolonged PD-L1 elimination via receptor crosslinking.

Previous studies have reported that adaptive PD-L1 up-regulation on disparate cellular sources, including tumor cells and tumor-infiltrating myeloid cells, non-redundantly modulate immunosuppression.[16] We further analyzed PD-L1 expression on tumor cells (CD45-), myeloid-derived suppressor cells (MDSCs, CD11b+GR1+), DCs (CD11c+F4/80-), and macrophages (CD11b+F4/80+).[16b] After KT-1 treatment, PD-L1 expression was profoundly increased in tumor cells, and slightly elevated on DCs and macrophages. The expression of PD-L1 on MDSCs did not change following KT-1 therapy, but MDSCs in saline-treated tumors already had a high basal level of PD-L1. Of note, sequential treatment with MPPA overcame adaptive PD-L1 enrichment on tumor cells, DCs, and macrophages in response to KT-1, and further reduced the PD-L1 expression in MDSCs (Figure 4F). These results suggest that MPPA is able to target and inhibit PD-L1 adaptively or innately expressed on both tumor cells and tumor-infiltrating myeloid cells.

In addition, KT-1 dominantly increased CD8+ T cell infiltration while additional α-PD-L1, PPA, or MPPA did not further enhance tumor infiltration of CD8+ T cells. In contrast, the presence of Tregs remained unaffected after treatment with KT-1 while the α-PD-L1 and PPA-mediated blockade of PD-L1, known to create or maintain the Treg population in tumors,[17] depleted Tregs (Figure 4G). Moreover, with the concomitant increase in CD8+ T cells and the largest decrease in Tregs, combination of KT-1 and MPPA resulted in a dramatically higher CD8+ T cells to Tregs ratio than observed in other treatments (Figure 4G)

2.4 KT-1 and MPPA combination results in a long-term antitumor antigen-specific memory of cured animals

To validate the *in vivo* therapeutic effect, syngeneic BALB/c mice bearing 4T1tumor were treated as shown in Figure 5A. Results in Figure 5B and Figure S8, Supporting Information showed that PPA barely delayed the tumor growth as compared with saline. MPPA exhibited slightly better therapeutic efficacy than PPA, probably due to the polymer-mediated effects of passive tumor targeting and PD-L1 crosslinking. However, the immunosuppressive tumor microenvironment failed to control the tumor progression at the endpoint. In contrast, combination therapies, KT-1→PPA and KT-1→MPPA, resulted in striking regression of tumors. Notably, KT-1→MPPA exerted the highest antitumor efficiency among all groups and completely eradicated 100% of tumors, suggesting KT-1 propagated an immunogenic tumor microenvironment for MPPA and unleashed its capability to activate antitumor immunity to kill cancer. In addition, no treatment group underwent significant loss in body weight, suggesting minimal toxicity (Figure 5C).

To test whether there is an establishment of immunologic memory, mice that experienced complete tumor regression (CR) of 4T1 tumors and 100% survival from KT-1→MPPA therapy (Figure 5D) were subcutaneously re-challenged with either 4T1 cells or an unrelated murine colon cancer cells CT26. As shown in Figure 5E, CR mice were resistant to 4T1 but

not to CT26, while both 4T1 and CT26 tumors grew rapidly in naive mice. Moreover, co-culture of peripheral blood mononuclear cells (PBMCs) isolated from CR mice with live 4T1 cells significantly expanded frequencies of tumor cell-reactive T cells (IFN-γ+CD8+) as compared with the co-cultures with CT26 cells whereas PBMCs from naive mice failed to generate this 4T1-specific response (Figure 5F).

In parallel, the CR mice cured after initial KT-1→MPPA treatment were re-challenged by administration of 4T1 cells from tail vein on day 50, the endpoint of the combination therapy. As demonstrated, all re-challenged mice survived by the end of additional 60 days (Figure 5G), and were lung-metastasis free (Figure 5H). On the contrary, 80% mice from naive control group died before day 40 with significant lung metastasis tumor nodules. Meanwhile, KT-1→MPPA resulted in a higher frequency of CD44+CD62L- memory effector CD8+ T cells in spleen than untreated control (Figure 5I), which revealed the establishment of durable immunity against tumor relapse. Based on our evidence, these encouraging results obtained from KT-1→MPPA combination therapy in immunosuppressive 4T1 tumor models could be attributed to its ability to "turn up the heat" on the anti-tumor immune status *via* a hierarchically "cold-warm-hot" transition as shown in Figure 5J. Because of the restoration of anti-cancer immunity and subsequent generation of tumor-specific immune memory, durable immunity against the same tumor type are established.

2.5 Anti-tumor and anti-metastatic effects of KT-1 and MPPA combination in subcutaneous CT26 and metastatic LLC-1 tumor models

We have also evaluated the reproducibility of our strategy in subcutaneous CT26 colon carcinoma and metastatic LLC-1 Lewis lung carcinoma tumor models that are poorly immunogenic.[5a,18] In murine colon carcinoma model of CT26 tumor cells syngeneic to BALB/c mice, monotherapy with α-PD-L1 or MPPA only exerted marginal effect in inhibiting tumor growth. Tumor progression was effectively limited during KT-1 treatment, but the residual tumors continued to develop after cessation of KT-1 chemotherapy. In contrast, KT-1 combined with α-PD-L1 or MPPA exerted durable suppression of tumor growth even after the treatment termination. Moreover, KT-1→MPPA further improved the anti-tumor efficacy, and outperformed KT-1→α-PD-L1 (20% complete tumor regression), leading to complete regression of established tumors in 60% of animals (Figure 6A). In addition, simultaneous administration with CD8-depleting antibodies drastically impaired the efficacy of KT-1→MPPA (Figure 6A), demonstrating an important engagement of CD8+ T cell response in the effects of the combination therapy. This is largely due to the modulation of KT-1, which, as expected, induced considerable exposure of surface CRT (Figure 6 B, C), one of the ICD hallmarks, and consequently stimulated a substantial increase in the ratio of CD8+ T cells to immunosuppressive Tregs (Figure 6D), thus improving antitumor immunity. However, residual tumor cells surviving from KT-1 treatment neutralized the elicitation of CD8+ T cell response by adaptively increasing the surface PD-L1 expression (Figure 6E). Notably, such dilemma could be overcome by sequential treatment with α-PD-L1 or MPPA. Furthermore, after KT-1 therapy, MPPA generated a more profound decrease in PD-L1 expression than α-PD-L1 (Figure 6E),

because MPPA exerted a more persistent effect on the suppression of surface PD-L1 recovery than α-PD-L1 (Figure 6F) as a result of receptor crosslinking.

Mice cured of the primary CT26 tumors with KT-1→MPPA therapy were re-challenged with the cancer cells of the same type. The growth of the secondary tumors in cured mice was significantly inhibited as compared with the primary tumors in naive mice (Figure 6G), indicating a long-term antitumor immune memory. Such protection against tumor relapse also caused a reshaped immune microenvironment in the secondary tumor with drastically increased population of infiltrated CD8+ T cells and slightly decreased population of immunosuppressive Tregs (Figure 6H). Interestingly, secondary tumor in cured mice generated a 2.5-fold greater upregulation of PD-L1 expression (Figure 6H), which could be one of the reasons for the failure of complete tumor regression, but could also mean an increased susceptibility to anti-PD-L1 immunotherapy especially when the tumor is substantially infiltrated by CD8+ T cells.

In LCC-1 carcinoma lung metastatic tumor model, C57BL/6 mice did not respond to immunotherapy of α-PD-L1 (median survival 24 days) or MPPA (median survival 28 days), with similar animal survival as saline-treated control (median survival 22 days), due to its immunogenic “cold” tumor status.[17] KT-1 alone (median survival 36 days) prolonged the survival of mice, but to a limited extent. While KT-1→α-PD-L1 (median survival 54 days) further extended animal survival, the best therapeutic outcome was achieved by KT-1→MPPA with significant improvement in mice median survival to 74 days (Figure 6I). Similarly, CD8 depletion abrogated the improvement made by KT-1→MPPA (Figure 6I), demonstrating the effect of KT-1→MPPA was CD8+ T cell-dependent. Indeed, mice that received treatment with KT-1, KT-1→α-PD-L1, or KT-1→MPPA significantly expanded reactive IFN-γ+CD8+ T cells against LLC-1 tumor cells in PBMCs (Figure 6J) and CD8+CD62L-CD44+ effector memory T cells that could elicit immediate protections by producing cytokines like IFN-γ in the spleen (Figure 6K). Meanwhile, none of the treatments with saline, α-PD-L1, or MPPA increased the number of IFN-γ+CD8+ or CD8+CD62L-CD44+ T cells beyond the basal level. These results confirmed that ICD-inducing conjugate KT-1 had a major effect on elicitation of broad anti-tumor immune response and anti-tumor immune memory. Furthermore, KT-1 combined with MPPA was more efficient in reducing the tumor burden and suppressing lung metastasis of LLC-1 cells than any other treatment (Figure 6L), meaning that PD-L1 crosslinking mediated by MPPA complemented the promoted anti-tumor immunity induced by KT-1.

3. Discussion

Chemotherapy is a widely used treatment for cancer, but after initial response many tumors frequently relapse and metastasize. One of the causes might be the sublethal accumulation of prescribed drugs in tumors. Recent evidence also suggests the residual tumor cells are able to evade the host immune system by increasing the surface PD-L1.[1] In current clinical trials, pre-existing chemotherapy has been complemented with concurrent PD-L1 blockade that restores T cell killing of targeted cells and provokes long-term immunological memory. However, durable remissions are only achieved in limited types of cancers invaded by swarms of pre-existing T cells.[2] Another challenge in PD-L1 blockade is that the

conformational binding between PD-L1 and prevalent anti-PD-L1 antibodies is reversible, and tumor cell surface is actively repopulated with recycled PD-L1 from cell interior.[8] These studies highlight the necessity of simultaneously (i) promoting tumoral T-cell immunity while (ii) inducing persistent PD-L1 suppression. Although combination strategies with immunogenic chemotherapy, [4,5] oncolytic virotherapy,[19] photothermal therapy,[20] and radiotherapy[3a] have been exploited to sensitize tumor to anti-PD-1/PD-L1 therapies with varying levels of success, majority of these studies only focus on the former issue while neglecting the latter.

In contrast, we here report the first proof-of-concept demonstration of polymer-assisted combination of improved immunogenic chemotherapy and prolonged PD-L1 degradation for efficacious treatment in originally non-immunogenic cancer: KT-1 conjugate efficiently targets EPI to tumors and enhances its direct anti-cancer activity as well as ICD induction, which, as a result, fosters tumor-specific CD8+ T cell response; MPPA conjugate crosslinks surface PD-L1 and directs PD-L1 to lysosomes for degradation. More importantly, in this game-changing battle against immunosuppressive cancer, we provide multiple lines of evidence indicating that KT-1 and MPPA collaboratively and hierarchically heat up immune-unresponsive tumor, *via* a “cold-warm-hot” immune status transition (Fig. 5I), thereby propagating a long-term antitumor immunity.

For instance, 4T1 tumors were initially “immune desert”: immunosuppressive Tregs seem to be preferentially recruited to the tumor site while CD8+ T cells are excluded from tumor microenvironment. With little immune engagement and no need to escape elimination, cell expression of PD-L1 checkpoint is low, representing another factor causing resistance to PD-L1 blockade. Second, KT-1 treatment warms the tumor by efficiently targeting immunogenic EPI drugs to tumor site. The subsequent induction of signals implicated in ICD makes tumor more prone to recognition by immune system, thus facilitating the recruitment of diverse CD8+ T cells to kill cancer cells. However, in order to escape detection and destruction by these immune effector cells, the residual 4T1 cells adaptively hijack checkpoints, such as PD-L1, and switch off T-cell response. Third, to flip the switch back on, MPPA not only targets and blocks surface PD-L1, but also crosslinks PD-L1, biases its recycling to lysosome degradation, and depletes it with increased vigor. The heightened activity of PD-L1 inhibition revives the slumbering T cells, accompanies the Tregs down-regulation, and thus further heats up tumor *via* spurring immune T cell responses.

Besides, in the other two immunosuppressive tumor models, CT26 colon carcinoma and metastatic LLC-1 lung carcinoma, similar therapeutic outcomes and “immunologically heating” mechanisms have also been observed after combination treatment of KT-1 and MPPA. Potent ICD induction by KT-1 significantly reshaped and promoted the anticancer immunity in those “cold” tumors, and reversed non-responding tumors to checkpoint therapy-responding ones. Subsequent therapy of MPPA launched a second-wave attack to crosslink the up-regulated PD-L1 for prolonged inhibition, cutting off the adaptive immune escape mechanism exploited by tumors reacting to KT-1 triggered tumor infiltration of CD8+ T cell. Owing to the eventual generation of antitumor immunity and T cell response memory in these heterogeneous tumors, KT-1 and MPPA combination is expected to be a generalizable and versatile platform to treat a broad spectrum of immunosuppressive tumors.

4. Conclusion

In summary, KT-1 and MPPA, with a rationale for combination therapy, provide a new, generalizable framework for using polymer-based nanomedicines to reprogram the immune microenvironment in immunologically “cold” tumor and empower the army of the immune system to fight cancer. Through polymer-enhanced tumor targeting, KT-1 effectively induces ICD *in vivo* and sensitizes tumors to checkpoint blockade. Relying on polymer-assisted multivalent binding, MPPA provides the first instance of using receptor crosslinking for controlled trafficking and lysosomal degradation of PD-L1. Because there is intense interest in applying immunotherapy to immunosuppressive cancers, our approach may be broadly transformative and expand the research of cancer therapy.

5. Experimental Section

Synthesis and Characterization

KT-1 (also known as 2P-EPI), backbone degradable HPMA copolymer – epirubicin (EPI) conjugate was synthesized *via* one step RAFT copolymerization of HPMA and *N*-(methacryloylglycylphenylalanylleucylglycyl)epirubicin (MA-GFLG-EPI) using VA044 as initiator and peptide2CTA (N^{α},N^{ε}-bis(4-cyano-4-(phenylcarbonothioylthio)pentanoyl-glycylphenylalanylleucylglycyl)lysine)[21] as chain transfer agent as previously reported.[7] For structure and characterization see Figure S1, Supporting Information. MPPA, backbone-degradable HPMA copolymer grafted with multiple copies of PD-L1 peptide antagonist PPA, was prepared via thiol-ene reaction as shown in Figure S1C, Supporting Information. Briefly, PPA (NYSKPTDRQYHF) was synthesized using Fmoc/tBu strategy and solid phase synthesis methodology on a PS3 peptide synthesizer. The sequence was appended with an N-terminal cysteine residue to obtain a thiol residue tagged peptide (PPA-Cys) for subsequent bioconjugation. The peptide structure was verified by MALDI-TOF mass spectrometry (PPA-Cys: calculated 1659.7 Da, found 1659.7 Da) and the purity of the peptide was verified with analytical RP-HPLC. HPMA copolymer precursor containing pendant amino groups (2P-NH_2) was prepared via RAFT copolymerization of HPMA with *N*-(3-aminopropyl)methacrylamide (APMA) using a bifunctional chain transfer agent Peptide2CTA. The dithiobenzoate end groups were removed by radical-induced end-modification using excess of V-65 in methanol at 55 °C. After precipitation into acetone and filtration, white powder was obtained, followed by dialysis (MWCO 6,000–8,000) against water over 16 h and lyophilization. Maleimide functionalized polymer precursor (2P-mal) was then obtained by reaction of 2P-NH_2 with a heterobifunctional reagent succinimidyl-4-(*N*-maleimidomethyl)cyclohexane-1-carboxylate (SMCC) in dimethylformamide in the presence of a tertiary amine (DIPEA) at room temperature for 2 h (molar ratio of [NH_2]:[SMCC]:[DIPEA]= 1:1.5:3). The maleimide content of the precursor was 22 maleimide groups per chain as measured by modified Ellman’s assay. PPA conjugation was achieved by attaching PPA-Cys to 2P-mal with the 1:1 molar ratio of PPA-Cys to maleimide to generate the multivalent polymer-peptide antagonist, MPPA. The reaction was performed in 10 mM PBS (pH 6.5) and kept stirring at room temperature for 3 h. At the end, unreacted PPA-Cys was removed by ultrafitration (30,000 Da cut-off) with 4 times DI water wash and freeze-dried. The average molecular weight and the polydispersity of the conjugates were

determined by SEC on an AKTA FPLC system equipped with a UV detector (GE Healthcare), miniDAWN TREOS and OptilabrEX (refractive index, RI) detector (Wyatt Technology) using a Superose 6 HR10/30 column with sodium acetate buffer containing 30% acetonitrile (pH 6.5) as mobile phase. The content of PPA in MPPA was determined using bicinchoninic acid (BCA) protein assay (Pierce).

Cell culture

4T1 cells (ATCC), CT26 cells (ATCC), and LLC-1 cells (ATCC) were maintained in in RPMI-1640 medium (Gibco) containing 10% fetal bovine serum (FBS) and a mixture of 0.1 mg/mL streptomycin and 100 units/mL penicillin at 37 °C in a humidified 5% CO_2 atmosphere.

Expression of CRT in vitro

Immunofluorescence analysis was used to evaluate the CRT expressions on 4T1 and CT26 cells before and after KT-1 treatment. Cells (2×10^5) were seeded in 4-well chamber. After 24 h incubation, cell culture medium was removed and cells were left untreated or treated with KT-1 (40 μM EPI equivalence) for 24 h to induce ICD. After the treatment, cells were washed with cold PBS, and further incubated with anti-CRT polyclonal antibody (1:100 dilution, Thermo Scientific) for 1 h at 37 °C. Cells were then washed with 1% BSA buffer twice and stained with Alexa Fluor 647 labeled goat anti-rabbit IgG (H+L) highly cross-adsorbed secondary antibody (1:200 dilution, Thermo Scientific) for 30 min at 4 °C. At the end, the nuclei were stained with 5 μg/mL Hoechst 33342 (Thermo Scientific) for 5 min, prior to confocal visualization.

Lysosome co-localization

4T1 cells (2×10^5) were seeded in 4-well chamber. After 24 h incubation, cell culture medium was removed and cells were treated with either Cy5 labeled α-PD-L1 (50 μg/mL) or Cy3 labeled MPPA (0.25 mg/mL) for 3 h at 37 °C. The lysosomes were stained with LysoTracker™ Green DND-26 (Thermo Scientific) at 37 °C for 15 min. Afterward cells were washed with PBS, prior to confocal visualization. Flow cytometry was also used to measure the fluorescent intensity of LysoTracker™ Green DND-26 labeled lysosome in 4T1 cells after 3 h treatments with α-PD-L1 antibody, PPA peptide, HPMA polymer backbone, and MPPA at 37 °C.

Whole cell PD-L1 expression after treatment with MPPA and partial inhibition of lysosomal enzymes

4T1 cells (2×10^5) were seeded in a 24-well plate. After 24 h incubation, cell culture medium was removed and cells were treated with fresh cell culture medium (untreated), α-PD-L1 (50 μg/mL, 10F.9G2), or MPPA (0.25 mg/mL) in the absence or presence of 20 μM E-64 (Sigma), an irreversible, potent, and highly selective cysteine protease inhibitor to partially prevent enzymatic lysosomal degradation, for 3 h at 37 °C. Afterward, cells were washed twice with PBS, and further incubated with fresh cell culture medium for 24 h at 37 °C. Then cells were detached, washed with cold PBS, fixed by 4% paraformaldehyde for 15 min at room temperature, permeabilized by 90% methanol for 30 min on ice, and immunostained

by Cy5-conjugated anti-PD-L1 antibody (1:200 dilution, MIH5) in 3% BSA buffer for 1 h at room temperature. After washing by cold PBS twice, the fluorescence was quantified by flow analysis. All experiments were carried out in triplicate.

Surface PD-L1 recycling

Recycling assay of internalized PD-L1 to cell surface was conducted following a previously established protocol. [8a] Briefly, cell surface was precoated with saturating concentrations of α-PD-L1 antibody (10F.9G2), PPA peptide, or MPPA conjugate at 4 °C for 2 h. Afterward, cells were washed with cold PBS twice to remove unbound antibody, peptide or conjugates. Internalization of surface binding formulations was allowed at 37 °C. At designated time points (0, 1, 3, 6, 24 h), surface accessible PD-L1 receptors were stained with Cy5-labeled α-PD-L1 antibody (MIH5) and measured by flow cytometry.

Animals

BABL/c mice and C57BL/6 mice were obtained from Charles River Laboratories. Mice were cared for following federal, state, and local guidelines. All work performed on animals was in accordance with and approved by the University Committee on Use and Care of Animals at the University of Utah, Salt Lake City. The animals were allowed free access to sterile food pellets and water.

In vivo tumor accumulation and cell uptake

4T1 cells (2×10^6) in 100 μL of PBS were implanted in the breast pad of 8-week-old female BABL/c mice. One week later, the mice were intravenously injected with 4 nmol of Cy5 or Cy5-labeled KT-1 and MPPA conjugate. At selected time points (2, 24, 72, 120, and 196 h after administration), imaging of whole body or excised organs was captured using the IVIS optical imaging system. For *in vivo* tumor cell uptake, 4T1 tumor bearing BALB/c mice were intravenously injected with free EPI or KT-1 (10 mg/kg EPI equivalence). At 1, 4, 7 day postinjection, mice (n=5) were sacrificed. Tumor tissues were collected and cut into small pieces, and tumor cells were dissociated in digestion buffer. The cell suspension was passed through a 70 μm nylon strainer, washed with PBS, incubated with ACK lysing buffer (room temperature, 5 min, Thermo Scientific) to remove red blood cells. After washed twice with cold PBS, tumor cells were suspended in PBS. The intracellular fluorescence of EPI was quantified using flow cytometry.

Immune status investigation

4T1 cells (2×10^6) in 100 μL of PBS were inoculated in the breast pad of 8-week-old female BABL/c mice on Day 0. CT26 cells (2×10^6) in 100 μL of PBS were subcutaneously injected in the right flank of 8-week-old female BABL/c mice on Day 0. LLC-1 cells (2×10^5) in 100 μL of PBS were intravenously injected into 8-week-old C57BL/6 mice on Day 0. For *in vivo* evaluation of ICD induction, tumor-bearing mice (n=4~6) were intravenously given two doses of saline, EPI or KT-1 (first EPI equivalence dose10 mg/kg followed by second dose 5 mg/kg) on Day 7 and Day 14. Afterward, mice were sacrificed on Day 15. For *in vivo* combination therapies, tumor bearing mice (n=5) were intravenously given two doses of KT-1 (first EPI equivalent dose 10 mg/kg followed by second dose 5 mg/kg) on Day 7 and

Day 14, followed by one dose of α-PD-L1 (100 μg per mouse), PPA, or MPPA (4 mg/kg PPA equivalent) on Day 15. Two days later, mice were sacrificed. Tumor tissues were collected. Single cell suspensions were prepared as described above. To stain the CD8+ T cells and Tregs, cell suspensions were fixed with 4% paraformaldehyde for 20 min and first incubated with 0.25 μg anti-CD16/32 antibody (4 °C, 20 min) to block the nonspecific Fc interaction, and then incubated with 1% BSA solution containing fluorescent-labeled primary antibodies (Biolegend) of anti-CD3-FITC (0.5 μg), anti-CD8-APC (0.25 μg), anti-CD4-PerCP (0.25 μg), or anti-Foxp3-PE (0.25 μg) at 4 °C for 60 min. Afterward, cells were washed and suspended in PBS for flow cytometry analysis. To measure the CRT expression, cell suspensions were incubated with anti-CRT polyclonal antibody (1:100 dilution) for 1 h at 37 °C. Then, cells were washed with 1% BSA buffer twice and stained with Alexa Fluor 647 labeled goat anti-rabbit IgG (H+L) highly cross-adsorbed secondary antibody (1:200 dilution) for 30 min at 4 °C. Afterward, cells were washed with cold PBS and re-suspended in PBS for flow cytometry analysis. The intratumoral concentration of HMGB1 in cell suspension before ACK lysing was measured using a mouse HMGB1 ELISA kit (LifeSpan BioSciences) after centrifugation and collecting the supernatant. To assess the activation of TIDCs (F4/80-CD11c+CD11b−/+), cells isolated from tumors were first incubated with 0.25 μg anti-CD16/32 antibody (4 °C, 20 min), and then incubated with 1% BSA solution containing fluorescent-labeled primary antibodies of anti-CD11c-FITC (0.25 μg), anti-CD11b-PE (0.25 μg), anti-F4/80-APC/Cy7 (0.25 μg), anti-MHC II-APC (0.25 μg) and anti-CD86-PerCP (0.25 μg) at 4 °C for 60 min. Afterward, cells were washed and suspended in PBS for flow cytometry analysis. To analyze PD-L1 expression on tumor cells (CD45-) and tumor-infiltrating myeloid cells including MDSCs (CD11b+GR1+), DCs (CD11c+F4/80-), and macrophages (CD11b+F4/80+), cells were blocked with anti-CD16/32 and then stained with antibodies against CD45, CD11b, CD11c, F4/80, PD-L1 as described above.

In vivo therapeutic efficacy

Tumor models were established as described above. Treatment schedules and dosages are provided in Supplementary files. The tumor volumes of mice were monitored thereafter. The tumor volume was calculated according to the following formula: $width^2 \times length \times 0.5$. The body weight and animal survival were recorded after the tumor implantation.

To test whether there is a specific establishment of immunologic memory, mice that experienced complete tumor regression (CR) from KT-1→MPPA combination treatment were s.c. rechallenged with either 4T1 cells (2×10^6) or CT26 (2×10^6) cells. As control groups, untreated naive mice were s.c. injected with 4T1 or CT26 cells. The tumor volumes for each group were measured. At the endpoint, mice were sacrificed, peripheral blood was collected, and peripheral blood mononuclear cells (PBMCs) was prepared in 10% FBS cell culture medium after lysing with ACK lysis buffer and 3 times PBS wash. PBMCs (10 million) were co-cultured with 0.1 million 4T1 cells, or CT26 cells at 37 °C for 18 h. Then, cells were washed twice with cold PBS and incubated with anti-CD16/32 antibodies (0.25 μg) at 4 °C for 20 min. After stained with anti-CD8-APC (0.25 μg) for 30 min at 4 °C, cells were washed and fixed with 4% paraformaldehyde for 10 min, followed by staining with interferon-γ (IFN-γ)-PE (0.25 μg) at room temperature for 30 min. Then cells were washed and suspended in PBS, prior to flow cytometry analysis.

To evaluate long-term antitumor memory of cured animals to inhibit metastatic lung tumor, CR mice (n=5) from KT-1→MPPA treatment were intravenously injected with 5×10^5 4T1 cells on day 50, the endpoint of the combination therapy. The survival was recorded thereafter. After mice died or were sacrificed at the endpoint, lung metastasis tumor nodules were counted and spleens were collected. Single-cell suspensions from spleens were stained with anti-CD8-APC, anti-CD62L-PerCP-Cy5.5 and anti-CD44-PE antibodies. Effector memory T cells, defined as CD62L-CD44+, were analyzed by flow cytometry (gated on CD8+T cells).

To evaluate the immune status and tumor burden in LLC-1 tumor-bearing mouse model, mice were sacrificed on Day 25 post tumor inoculation. Reactive IFN-γ+CD8+ among PBMCs against LLC-1 cells and CD44+CD62L- memory effector CD8+ T cells in spleen were analyzed as described above. Lung weight, a proxy of tumor burden, was measured. Tumor metastasis in lung lobe was analyzed using hematoxylin-eosin histology.

Supplementary Material

Refer to Web version on PubMed Central for supplementary material.

Acknowledgements

The research was supported in part by NIH grant R42 CA156933, TheraTarget, and J.K.'s development funds. We acknowledge support of funds in conjunction with grant P30 CS042014 awarded to Huntsman Cancer Institute and to the ET Program at Huntsman Cancer Institute.

References

[1]. a)Samanta D, Park Y, Ni X, Li H, Zahnow CA, Gabrielson E, Pan F, Semenza GL, Proc. Natl. Acad. Sci. U. S. A. 2018, 115, 1239;b)Peng J, Hamanishi J, Matsumura N, Abiko K, Murat K, Baba T, Yamaguchi K, Horikawa N, Hosoe Y, Murphy SK, Konishi I, Cancer Res. 2015, 75, 5034; [PubMed: 26573793] c)Haratake N, Toyokawa G, Tagawa T, Kozuma Y, Matsubara T, Takamori S, Akamine T, Yamada Y, Oda Y, Maehara Y, Anticancer Res. 2017, 37, 5713. [PubMed: 28982891]

[2]. a)Tumeh PC, Harview CL, Yearley JH, Shintaku IP, Taylor EJM, Robert L, Chmielowski B, Spasic M, Henry G, Ciobanu V, West AN, Carmona M, Kivork C, Seja E, Cherry G, Gutierrez AJ, Grogan TR, Mateus C, Tomasic G, Glaspy JA, Emerson RO, Robins H, Pierce RH, Elashoff DA, Robert C, Ribas A, Nature 2014, 515, 568; [PubMed: 25428505] b)Sato E, Olson SH, Ahn J, Bundy B, Nishikawa H, Qian F, Jungbluth AA, Frosina D, Gnjatic S, Ambrosone C, Kepner J, Odunsi T, Ritter G, Lele S, Chen Y-T, Ohtani H, Old LJ, Odunsi K, Proc. Natl. Acad. Sci. U.S.A. 2005, 102, 18538; [PubMed: 16344461] c)Rizvi NA, Hellmann MD, Snyder A, Kvistborg P, Makarov V, Havel JJ, Lee W, Yuan J, Wong P, Ho TS, Miller ML, Rekhtman N, Moreira AL, Ibrahim F, Bruggeman C, Gasmi B, Zappasodi R, Maeda Y, Sander C, Garon EB, Merghoub T, Wolchok JD, Schumacher TN, Chan TA, Science 2015, 348, 124; [PubMed: 25765070] d)Schumacher TN, Schreiber RD, Science 2015, 348, 69. [PubMed: 25838375]

[3]. a)Duan X, Chan C, Lin W, Angew. Chem. Int. Ed. 2019, 58, 670;b)Green DR, Ferguson T, Zitvogel L, Kroemer G, Nat. Rev. Immunol. 2009, 9, 353; [PubMed: 19365408] c)Galluzzi L, Buqué A, Kepp O, Zitvogel L, Kroemer G, Nat. Rev. Immunol. 2016, 17, 97; [PubMed: 27748397] d)He C, Duan X, Guo N, Chan C, Poon C, Weichselbaum RR, Lin W, Nat. Commun. 2016, 7, 12499. [PubMed: 27530650]

[4]. a)Obeid M, Tesniere A, Ghiringhelli F, Fimia GM, Apetoh L, Perfettini J-L, Castedo M, Mignot G, Panaretakis T, Casares N, Métivier D, Larochette N, van Endert P, Ciccosanti F, Piacentini M, Zitvogel L, Kroemer G, Nat. Med. 2006, 13, 54; [PubMed: 17187072] b)Apetoh L, Ghiringhelli

F, Tesniere A, Obeid M, Ortiz C, Criollo A, Mignot G, Maiuri MC, Ullrich E, Saulnier P, Yang H, Amigorena S, Ryffel B, Barrat FJ, Saftig P, Levi F, Lidereau R, Nogues C, Mira J-P, Chompret A, Joulin V, Clavel-Chapelon F, Bourhis J, André F, Delaloge S, Tursz T, Kroemer G, Zitvogel L, Nat. Med. 2007, 13, 1050; [PubMed: 17704786] c)Ma Y, Adjemian S, Mattarollo SR, Yamazaki T, Aymeric L, Yang H, Portela Catani JP, Hannani D, Duret H, Steegh K, Martins I, Schlemmer F, Michaud M, Kepp O, Sukkurwala AQ, Menger L, Vacchelli E, Droin N, Galluzzi L, Krzysiek R, Gordon S, Taylor PR, Van Endert P, Solary E, Smyth MJ, Zitvogel L, Kroemer G, Immunity 2013, 38, 729; [PubMed: 23562161] d)Pfirschke C, Engblom C, Rickelt S, Cortez-Retamozo V, Garris C, Pucci F, Yamazaki T, Poirier-Colame V, Newton A, Redouane Y, Lin Y-J, Wojtkiewicz G, Iwamoto Y, Mino-Kenudson M, Huynh TG, Hynes RO, Freeman GJ, Kroemer G, Zitvogel L, Weissleder R, Pittet MJ, Immunity 2016, 44, 343. [PubMed: 26872698]

[5]. a)Kuai R, Yuan W, Son S, Nam J, Xu Y, Fan Y, Schwendeman A, Moon JJ, Sci. Adv. 2018, 4, eaao1736;b)Li L, Sun W, Zhong J, Yang Q, Zhu X, Zhou Z, Zhang Z, Huang Y, Adv. Funct. Mater. 2015, 25, 410.

[6]. a)Šírová M, Strohalm J, Šubr V, Plocová D, Rossmann P, Mrkvan T, Ulbrich K, Říhová B, Cancer Immunol. Immunother. 2007, 56, 35; [PubMed: 16636810] b)Říhová B, Kovář L, Kovář M, Hovorka O, Trends Biotechnol. 2009, 27, 11. [PubMed: 19022512]

[7]. a)Zhang R, Yang J, Sima M, Zhou Y, Kopeček J, Proc. Natl. Acad. Sci. U. S. A. 2014, 111, 12181; [PubMed: 25092316] b)Yang J, Zhang R, Radford DC, Kopeček J, Controlled Release J 2015, 218, 36;c)Zhang L, Zhang R, Yang J, Wang J, Kopeček J, Controlled Release J 2016, 235, 306;d)Yang J, Kopeček J, Curr. Opin. Colloid Interface Sci. 2017, 31, 30. [PubMed: 29276426]

[8]. a)Burr ML, Sparbi er CE, Chan Y-C, Williamson JC, Woods K, Beavis PA, Lam EYN, Henderson MA, Bell CC, Stolzenburg S, Gilan O, Bloor S, Noori T, Morgens DW, Bassik MC, Neeson PJ, Behren A, Darcy PK, Dawson S-J, Voskoboinik I, Trapani JA, Cebon J, Lehner PJ, Dawson MA, Nature 2017, 549, 101; [PubMed: 28813417] b)Wang H, Yao H, Li C, Shi H, Lan J, Li Z, Zhang Y, Liang L, Fang J-Y, Xu J, Nat. Chem. Biol. 2019, 15, 42; [PubMed: 30397328] c)Yao H, Lan J, Li C, Shi H, Brosseau J-P, Wang H, Lu H, Fang C, Zhang Y, Liang L, Zhou X, Wang C, Xue Y, Cui Y, Xu J, Nat. Biomed. Eng. 2019, 3, 306. [PubMed: 30952982]

[9]. a)Moody PR, Sayers EJ, Magnusson JP, Alexander C, Borri P, Watson P, Jones AT, Mol. Ther. 2015, 23, 1888; [PubMed: 26412588] b)Li L, Yang J, Wang J, Kopeček J, Macromol. Biosci. 2018, 18, 1700196;c)Li L, Yang J, Soodvilai S, Wang J, Opanasopit P, Kopeček J, J. Controlled Release 2019, 293, 84.

[10]. a)Johnson RN, Kopečková P, Kopeček J, Biomacromolecules 2012, 13, 727;b)Wu K, Liu J, Johnson RN, Yang J, Kopeček J, Angew. Chem. Int. Ed. 2010, 49, 1451;c)Chu T-W, Yang J, Zhang R, Sima M, Kopeček J, ACS Nano 2014, 8, 719.

[11]. a)Li L, Yang J, Wang J, Kopeček J, ACS Nano 2018, 12, 3658;b)Li L, Wang J, Li Y, Radford DC, Yang J, Kopeček J, ACS Nano 2019, 13, 11422.

[12]. Preynat-Seauve O, Schuler P, Contassot E, Beermann F, Huard B, French LE J. Immunol. 2006, 176, 61. [PubMed: 16365396]

[13]. Spranger S, Spaapen RM, Zha Y, Williams J, Meng Y, Ha TT, Gajewski TF, Sci. Transl. Med. 2013, 5, 200ra116.

[14]. Chang H-N, Liu B-Y, Qi Y-K, Zhou Y, Chen Y-P, Pan K-M, Li W-W, Zhou X-M, Ma W-W, Fu C-Y, Qi Y-M, Liu L, Gao Y-F, Angew. Chem. Int. Ed. 2015, 54, 11760.

[15]. Perez-Balderas F, van Kasteren SI, Aljabali AAA, Wals K, Serres S, Jefferson A, Sarmiento Soto M, Khrapitchev AA, Larkin JR, Bristow C, Lee SS, Bort G, De Simone F, Campbell SJ, Choudhury RP, Anthony DC, Sibson NR, Davis BG, Nat. Commun. 2017, 8, 14254. [PubMed: 28198362]

[16]. a)Lau J, Cheung J, Navarro A, Lianoglou S, Haley B, Totpal K, Sanders L, Koeppen H, Caplazi P, McBride J, Chiu H, Nat. Commun. 2017, 8, 14572; [PubMed: 28220772] b)Deng L, Liang H, Burnette B, Beckett M, Darga T, Weichselbaum RR, X Fu Y, J. Clin. Invest. 2014, 124, 687. [PubMed: 24382348]

[17]. a)Munn DH, J. Clin. Invest. 2018, 128, 570; [PubMed: 29337304] b)Wang T, Wang D, Yu H, Feng B, Zhou F, Zhang H, Zhou L, Jiao S, Li Y, Nat. Commun. 2018, 9, 1532. [PubMed: 29670088]

[18]. Viitala M, Virtakoivu R, Tadayon S, Rannikko J, Jalkanen S, Hollmén M, Clin. Cancer Res. 2019, 25, 3289. [PubMed: 30755440]

[19]. Ribas A, Dummer R, Puzanov I, VanderWalde A, Andtbacka RHI, Michielin O, Olszanski AJ, Malvehy J, Cebon J, Fernandez E, Kirkwood JM, Gajewski TF, Chen L, Gorski KS, Anderson AA, Diede SJ, Lassman ME, Gansert J, Hodi FS, Long GV, Cell 2017, 170, 1109. [PubMed: 28886381]

[20]. Chen Q, Xu L, Liang C, Wang C, Peng R, Liu Z, Nat. Commun. 2016, 7, 13193. [PubMed: 27767031]

[21]. Pan H, Yang J, Kopečková P, Kopeček J, Biomacromolecules 2011, 12, 247. [PubMed: 21158387]

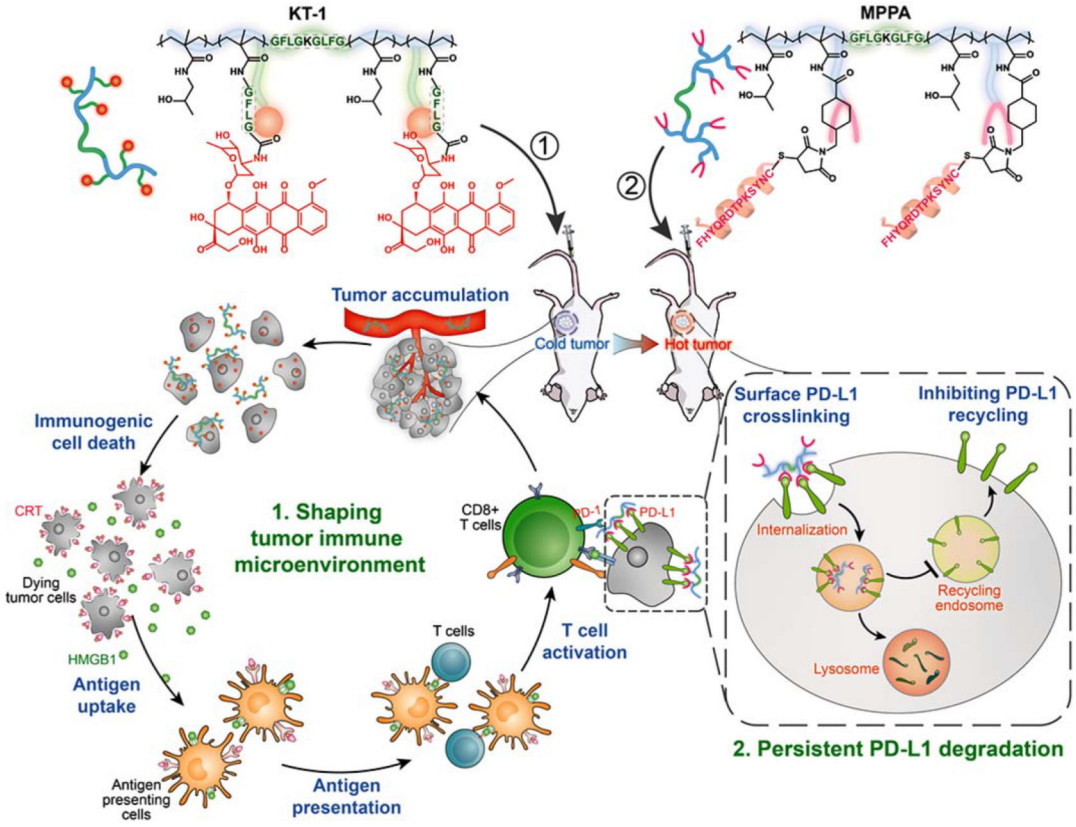

Figure 1. Schematic illustration of polymer-enhanced combination of immunogenic chemotherapy and PD-L1 degradation.

Backbone-degradable HPMA copolymer facilitates tumor targeting of immunogenic drug to enhance its direct antitumor activity as well as induction of ICD to “heat up” the antitumor immunity. Meanwhile, the copolymer also mediates the surface crosslinking of PD-L1, biases its recycling to lysosome degradation, and exhibits persistent suppression. This two-pronged approach recruits and revives the slumbering T cells in tumors and spurs T cell responses durably.

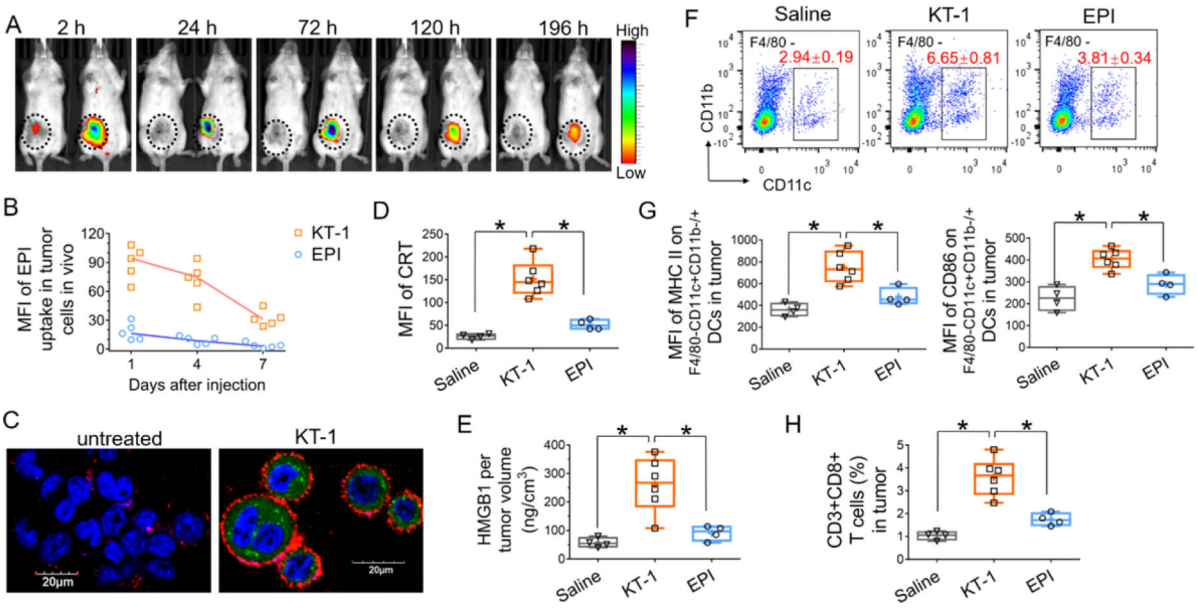

Figure 2. KT-1 mediated tumor accumulation and immunogenic cell death induction.

(A) Real-time fluorescence imaging of 4T1 tumor-bearing BALB/c mice (n=3) treated with Cy5 (left) and Cy5-labeled KT-1 (right) at 2, 24,72, 120, and 196 h after intravenous injection. Fluorescence intensities were normalized to the same scale. Black circles indicate the tumor. (B) *In vivo* tumor cell uptake of EPI at day 1, 4, 7 after the mice were treated with either free EPI or KT-1 (10 mg/kg EPI equivalent, n=5). (C) Confocal imaging of KT-1-enhanced CRT exposure on the surface of 4T1 cells *in vitro*. Blue: cell nuclei; Green: EPI; Red: CRT. (D) *In vivo* CRT up-regulation on tumor cell surface, (E) Intratumoral HMGB1 release, (F) Frequency of F4/80-CD11c+CD11b−/+ TIDCs, (G) activation status of TIDCs, and (H) CD8+ T cell infiltration in tumors after two dose treatments (on Day 7 and Day 14) of 4T1 tumor-bearing mice with saline, EPI and KT-1. Data are represented as box plots (whiskers, 5th to 95th percentile). n=4 for saline and EPI treatments, and n=6 for KT-1 treatment, **P*<0.05 by Student's *t*-test.

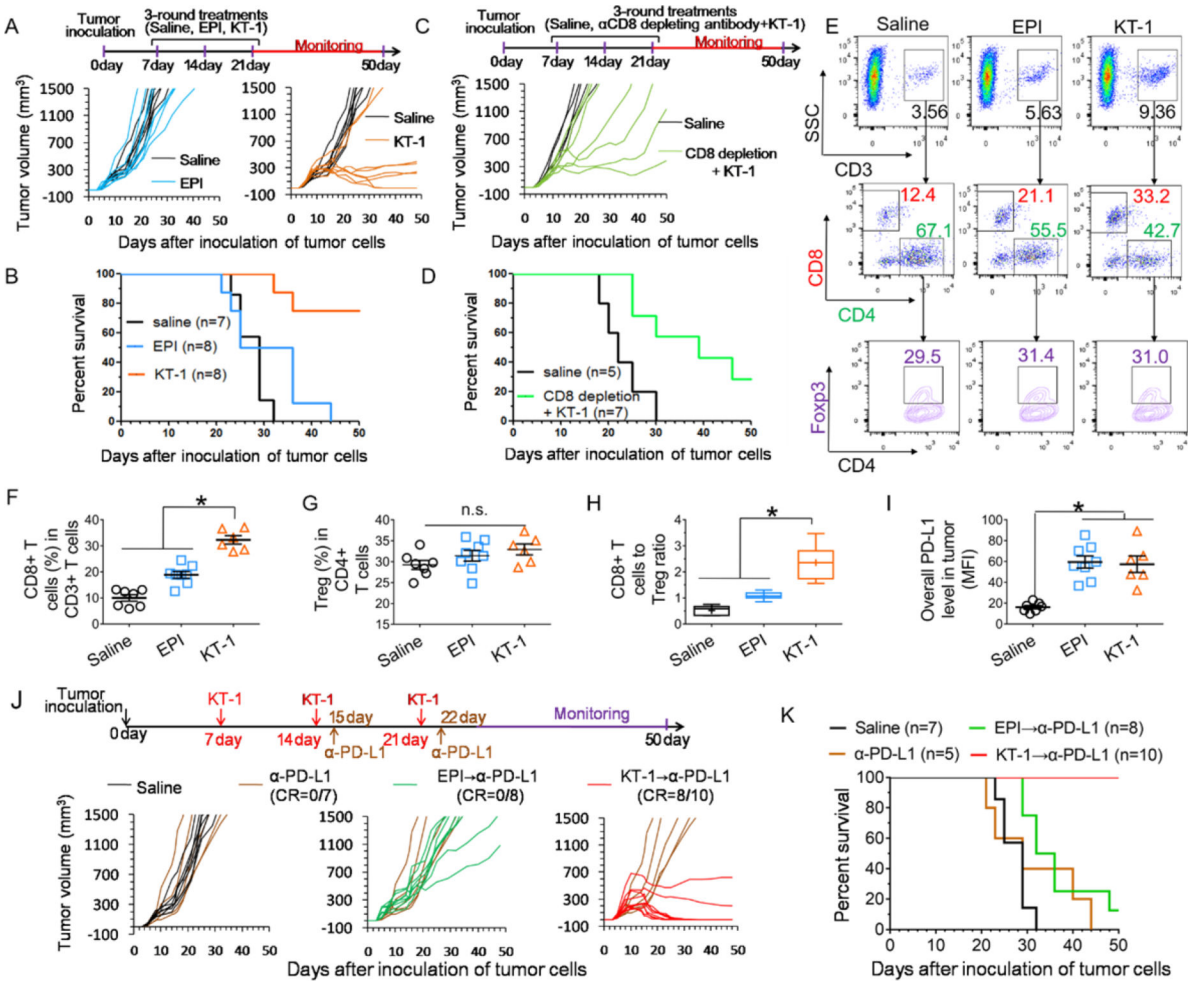

Figure 3. KT-1 improves *in vivo* outcomes in a CD8+ T cell-dependent manner and leads to adaptive enrichment of tumor PD-L1 expression.

(A) Individual tumor growth curves and (B) animal survival rate over time after treatments with saline, EPI and KT-1. The arrows indicate the treatment regimens. (C) Individual tumor growth curves and (D) animal survival rate over time after co-treatment with CD8-depleting antibodies and KT-1. The arrows indicate the treatment regimens. (E) Flow cytometry scatter plot representation of CD8+ T cells and CD4+Foxp3+ Tregs, and statistics of (F) tumor recruitment of CD8+ T cells, (G) Tregs, (H) CD8+ T cells to Treg ratio, and (I) PD-L1 expressions within tumor cells after chemotherapy with EPI and KT-1 indicated in (A). (J) Individual tumor growth curves and (K) animal survival rate over time after saline, EPI, and KT-1 treatments in combination with α-PD-L1. The arrows indicate the treatment regimens. CR, complete tumor regression. n=5–10, *P< 0.05, n.s., not significant, one-way ANOVA with Tukey's multiple comparison test, box plots represent whiskers, 5th to 95th percentile.

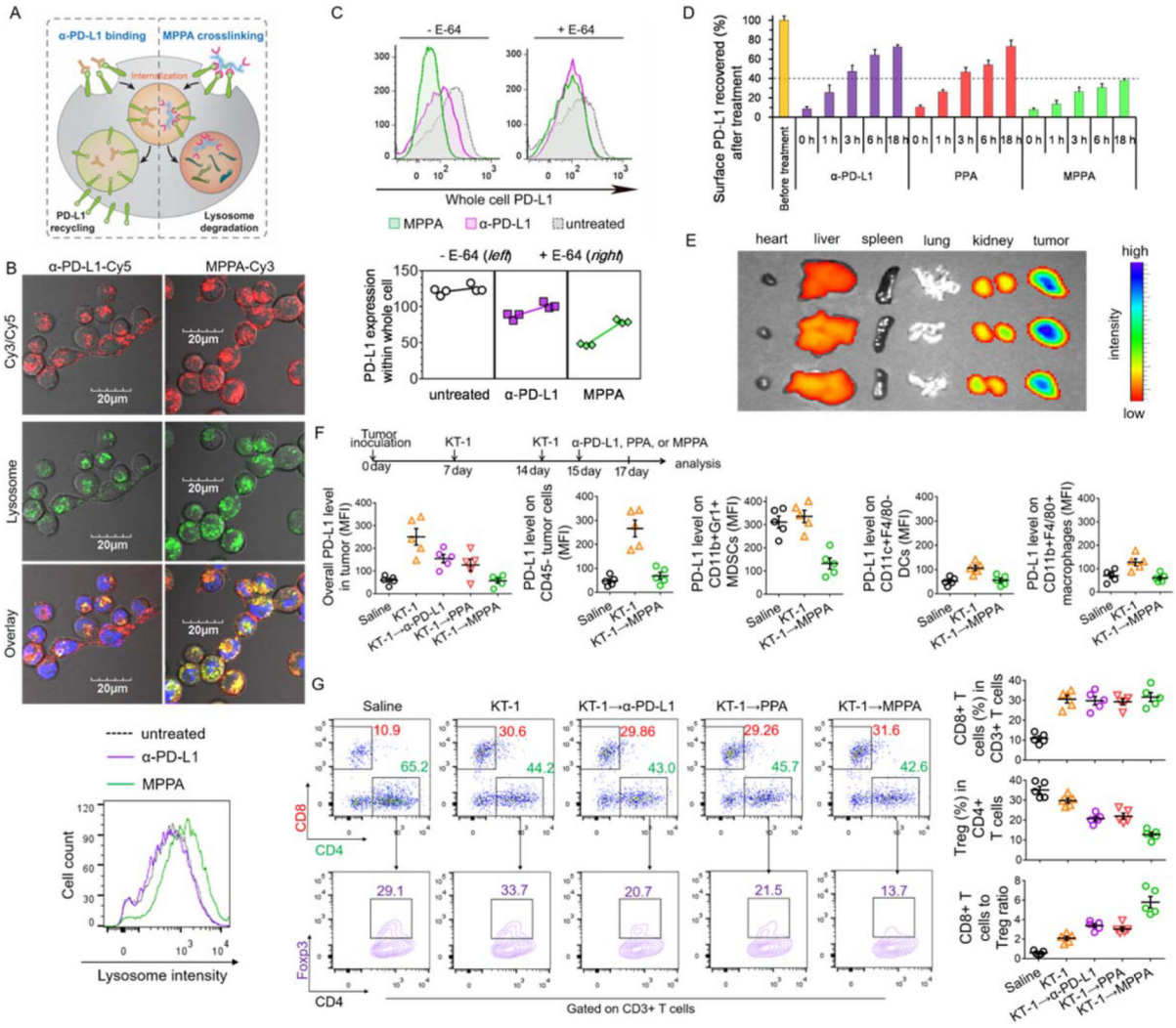

Figure 4. Crosslinking surface PD-L1 by MPPA directs PD-L1 to lysosomal degradation.

(A) Schematic illustration of inhibiting PD-L1 recycling by MPPA crosslinking. (B) Lysosome colocalization of α-PD-L1-Cy5 or Cy3-labeled MPPA (P-(PPA)14-Cy3) and lysosome intensity evaluation after 3 h treatment at 37 °C. Blue: nuclei; Red: Cy3/Cy5; Green: lysosomes. (C) Whole cell PD-L1 expression with or without lysosome hydrolysis inhibition by E-64. 4T1 cells were treated with α-PD-L1, PPA, or MPPA for 3 h in the absence (−) or presence (+) of E-64 cysteine protease inhibitor. Afterward, cells were further incubated in cell culture medium for another 24 h, prior to PD-L1 quantification. (D) Time-dependent recovery of surface PD-L1 after treatments with α-PD-L1, PPA, or MPPA. 4T1 cell surface was precoated with saturating concentration of antibody, peptide, or conjugates at 4 °C for 2 h. Then cells were washed and incubated with fresh cell culture medium at 37 °C. At selected time points (0, 1, 3, 6 h), surface accessible PD-L1 receptors were stained with fluorophore-labeled anti-PD-L1 antibody and measured by flow cytometry. (E) Biodistribution of MPPA-Cy5 in major organs in mice after 24 h post iv injection (n=3). (F) PD-L1 level on CD45- tumor cell, CD11b+GR1+ MDSCs, CD11c+F4/80- DCs, and CD11b +F4/80+ macrophages, and (G) analysis of CD8+ T cells and CD4+Foxp3+ Tregs in tumors

after KT-1 and MPPA combination treatment as indicated by arrows in (E). n=3 in (C) and (D), and n=5 in (E) and (F).

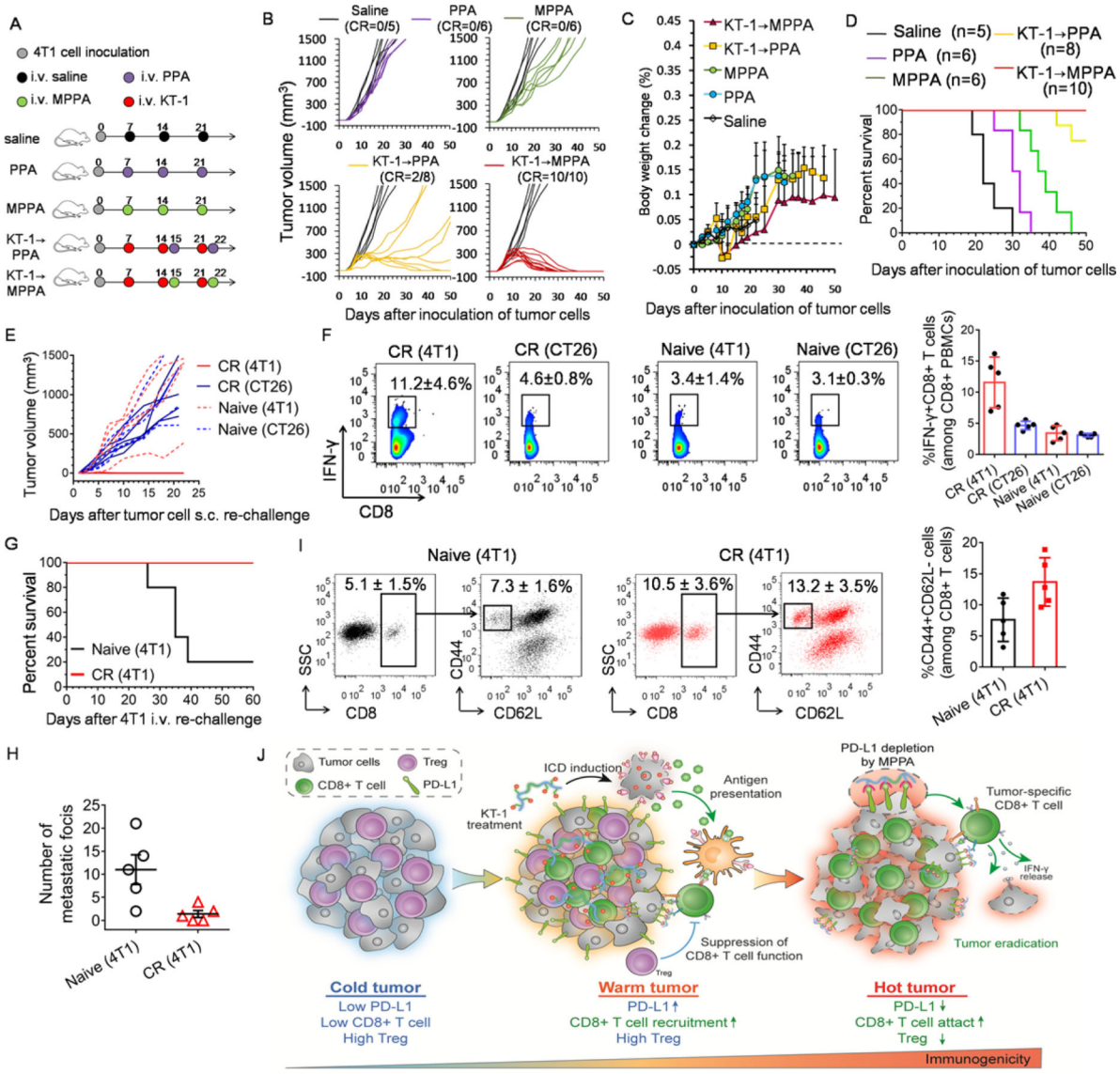

Figure 5. KT-1 and MPPA combination results in a long-term antitumor antigenic-specific memory of cured animals.

(A) Treatment schedules for the indicated treatments. (B) Individual tumor volumes, (C) body weight change, and (D) survival rate in 4T1-tumor bearing BALB/c mice over time after different treatments (n=5–10). (E) Individual tumor volumes after naive control mice or KT-1→MPPA treated CR mice from (D) were subcutaneously re-challenged with 4T1 or CT26 cells (n=5). (F) Representative scatter plots of the percentage of tumor cell-reactive T cells (IFN-γ+CD8+) among PBMCs from KT-1→MPPA treated CR mice from (D) against 4T1 cells and CT26 cells (n=5). (G) Mice survival curve after re-challenge by iv injection of 4T1 cells after initial KT-1→MPPA treatment (n=5). (H) Lung metastasis after BALB/c mice, implanted with 4T1 tumors and completely cured after initial KT-1→MPPA treatment, were re-challenged by iv injection of 4T1 cells. (I) CD44+CD62L- memory effector CD8+ T cells in the spleen after 4T1 cell re-challenge (n=5). (J) Schematic

illustration of “turning up the heat” on tumor immune status by KT-1 and MPPA combination treatment.

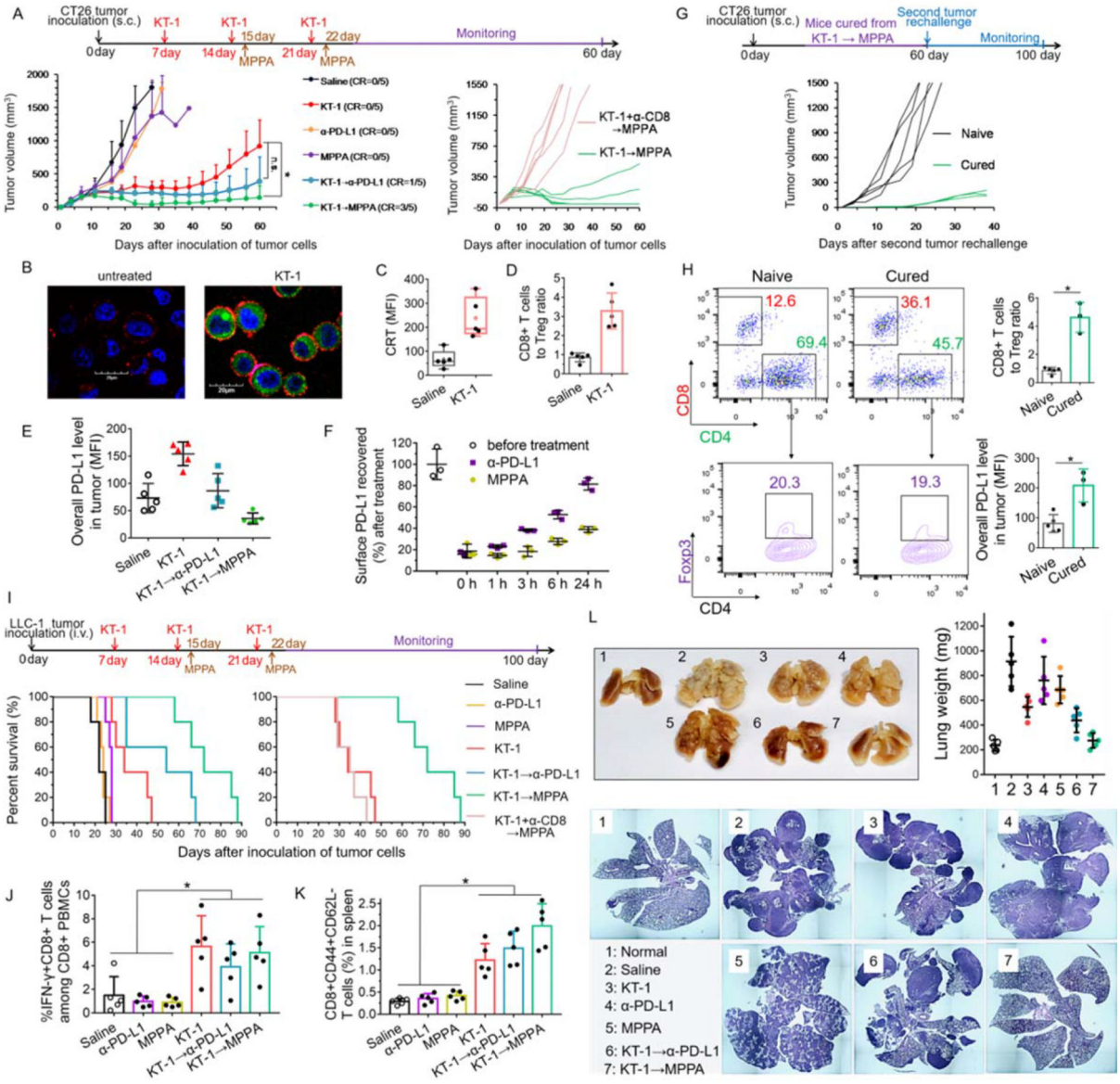

Figure. 6. Anti-tumor and anti-metastatic effects of KT-1 and MPPA combination in subcutaneous CT26 and metastatic LLC-1 tumor models.

(A) CT26 colon tumor growth curves after indicated treatments (n=5). BALB/c mice were subcutaneously inoculated with 2×10^6 CT26 cells on day 0. On days 7, 14, and 21, tumor-bearing mice were treated with KT-1. On days 15, and 22, mice were treated with anti-PD-L1 therapy, α-PD-L1 antibodies or MPPA conjugates. CD8-depleting antibodies were given simultaneously with KT-1 to mice subjected to CD8+ T-cell ablation. The arrows indicate the treatment regimens for KT-1 and MPPA combination. (B) Confocal images of KT-1-enhanced CRT exposure on the surface of CT26 cells *in vitro*. Blue: cell nuclei; Green: EPI; Red: CRT. *In vivo* (C) CRT up-regulation on cell surface, and (D) CD8+ T cells to Treg ratio, after two doses treatments (on Day 7 and Day 14) with saline and KT-1 for CT26 tumor-bearing mice. (E) *In vivo* PD-L1 expressions in CT26 tumors (on Day 17) after two doses treatment (on Day 7 and Day 14) with KT-1, followed by one dose (Day 15) treatment

with α-PD-L1 or MPPA. (F) Time-dependent recovery of surface PD-L1. CT26 tumor cells were isolated from tumor-bearing mice after two doses treatment (on Day 7 and Day 14) with KT-1. Then cell surface was precoated with saturating concentration of α-PD-L1 or MPPA at 4 °C for 2 h. Afterward, cells were washed and incubated with fresh culture medium at 37 °C. At selected time points (0, 1, 3, 6, 24 h), surface accessible PD-L1 receptors were stained with fluorophore-labeled anti-PD-L1 antibody and measured by flow cytometry. (G) Individual tumor volume measurement after naive control mice (n=5) or KT-1→MPPA treated CR mice (n=3) in (A) were subcutaneously re-challenged with CT26 cells. (H) Immune status including CD8+ T cells, Tregs, PD-L1 expression in primary CT26 tumors of naive mice and secondary CT26 tumors of cured mice. (I) Survival rate of mice after indicated treatments (n=5). C57BL/6 mice were intravenously inoculated with 2×10^5 LLC-1 Lewis lung carcinoma cells on day 0. Then mice were treated as described in (A). (J) Percentage of tumor cell-reactive T cells (IFN-γ+CD8+) among PBMCs against LLC-1 cells, (K) CD44+CD62L- memory effector CD8+ T cells in spleen, and (L) Tumor burden in lungs depicted as lung weight and hematoxylin-eosin histology analysis of lung lobe sections, from mice in (I) on Day 25 or their endpoint,. *P < 0.05, n.s, not significant, one-way ANOVA with Tukey’s multiple comparison test.